STRESS DISTRIBUTIONS IN FUEL ELEMENT CLADDING DURING PELLET-CLAD INTERACTION

R. S. DARLING, I. B. FIERO, M. E. SCOTT
Combustion Engineering, Inc.,
1000 Prospect Hill Road, Windsor, Connecticut 06095, U.S.A.

SUMMARY

The purpose of this paper is to quantify localized stresses, strains and clad ridging resulting from mechanical interaction of UO_2 fuel pellets with Zircaloy cladding during power ramps. Stress and strain concentrations occur in the clad adjacent to pellet cracks and pellet-pellet interfaces and may cause permanent clad ridging.

Pellet-clad mechanical interaction (PCMI) has been modeled over a broad range of conditions using the finite element code ANSYS. Stresses, strains, and clad ridging were determined over the range of 6 to 16 kw/ft and with pellet-clad gaps of from 1 to 5 mils. Clad ridging effects at the pellet-pellet interface and at pellet transverse cracks were analyzed using a two-dimensional axisymmetric pellet-clad model (R-Z). Additional clad stretching and bending adjacent to pellet radial cracks were analyzed using a two-dimensional plane section across the pellet (R-θ). Friction effects and axial interaction of pellet and clad were considered in both models. Plastic behavior of the fuel and clad were included. Power dependent crack patterns in the pellet were determined analytically based on UO_2 fracture strength. Thermal analyses were performed independent of the structural analyses.

Results from the R-Z model show that the fuel pellet cracks transversely (R-θ plane) near the midplane. Clad ridges develop at the pellet-pellet interface (primary ridging) and at the midplane crack (secondary ridging). These ridges increase in height with increasing linear heat rate (LHR) up to 11 to 15 kw/ft, and then decrease. Secondary ridge heights can exceed primary ridge heights. Peak ridge heights tend to be larger for larger initial pellet-clad gaps due to greater pellet distortion before contact. However, a greater ridge height, measured as relative clad displacement, does not necessarily give higher clad stress. The pellet can distort less but still induce large uniform mechanical interferences and stresses in the clad. Much of this predicted ridge height behavior has been observed in experimental data.

Clad hoop stresses and strains on the clad inner surface increase linearly with LHR until fuel softening from temperature effects starts slowing the rate of increase. Stresses and strains always increase with decreasing initial gap size over the entire LHR range.

Maximum hoop stress in the ridged clad occurs near the pellet-pellet interface. Concentration factors, defined as maximum over average, range from 3.0-5.0 at initial contact and decrease to 1.0-2.0 at 16 kw/ft. Hoop strains behave similarly. Ridging is insensitive to pellet-clad friction.

Results from the R-θ model show that peak clad stresses occur directly opposite radial cracks and decrease rapidly away from the crack. Consequently, the peak stress is independent of the number of radial cracks. Results are sensitive to friction. Stresses increase nearly linearly with increasing LHR and decrease with increasing initial gap. However, the concentration factor is insensitive to gap size.

Interesting new conclusions as a result of the analyses are:

1. Secondary ridges can exceed primary ridges
2. Ridging is larger for larger gaps
3. Ridge heights are not good indicators of peak stress
4. Numbers of radial fuel cracks do not significantly affect peak stresses

INTRODUCTION

Circumferential ridges have been observed in the cladding of water reactor fuel rods following irradiation and/or power ramps (e.g., ref. 1) with heights typically 0.5 to 2 mils (ridge height = maximum clad diameter minus minimum clad diameter). These ridges appear to occur adjacent to fuel pellet interfaces and, under certain conditions, at pellet midsections. The presence of these clad ridges demonstrates localized pellet-clad mechanical interaction phenomena. These phenomena are not generally addressed by typical fuel analyses which treat fuel and clad as essentially infinite cylinders.

Localized pellet-clad interactions can result from "hourglassing" and cracking of the fuel pellets at power. Many investigators (e.g., ref. 2) are now attempting to treat various aspects of these interactions between such hourglassed, cracked pellets and the clad.

In the present study (based on ref. 3), a large general purpose finite-element code (ANSYS) has been used to model both pellet and clad in detail, including thermal and cracking phenomena in the pellet, and the various radial, axial, and circumferential load distributions between pellet and clad during contact. Some simplification was considered appropriate. Most time dependent phenomena (swelling, hot-pressing, etc.) are not modeled, the idea being that these are adequately described on an average basis by the infinite cylinder codes. Fuel creep can significantly alter stress distributions in a relatively short time. Hence, fuel creep was modeled using isochronous creep curves.

The purpose of this study is to quantify by means of analytically derived concentration factors the stress (strain) localization occurring in the clad during pellet-clad mechanical interaction (PCMI). Such concentration factors could, if desired, be applied to fuel performance codes through appropriate common parameters or functional forms built into the codes.

DESCRIPTION OF MODELS

Localized clad stresses (strains) due to fuel pellet hourglassing and cracking have been quantitatively and systematically evaluated using two finite element models. Transverse pellet cracks (perpendicular to the centerline) are often observed and can be predicted on the bases of thermal stresses induced by the thermal gradients. Local clad stresses adjacent to these transverse cracks and at pellet interfaces are modeled with an axisymmetric two-dimensional model (R-Z). Additional clad stretching and bending adjacent to pellet radial cracks were analyzed using a two-dimensional plane section across the pellet (R-θ). Friction and axial interaction of pellet and clad were considered in both models. Plastic behavior of the fuel and clad were simulated using the method of isochronous creep curves. Power dependent crack patterns in the pellet were determined analytically based on UO_2 fracture strength. Thermal analysis, performed separately from the structural analysis, provided temperature gradients and allowed evaluation of temperature dependent properties. A brief description of the models and methods of analysis is given below.

R-Z model - The 2-dimensional R-Z model is shown in Fig. 1. It represents an unchamfered pellet typical of PWR designs. The finite element mesh consists of 365 ring elements and 40 gap/friction elements. The fuel consists of constant strain elements and the clad consists of isoparametric elements. This geometry remained fixed except for gap size which was parametrically varied. Temperature distributions were first established using a constant gap conductance (typical of contact conditions) and a fixed clad surface temperature. Iterative structural analysis, neglecting the clad, then provided stress distributions which, when compared with UO_2 fracture stress (assumed at 20 ksi), provided crack distributions in the pellet at various heat generation rates. It was then assumed that the appropriate crack pattern for a given gap size was that corresponding to the heat rate at which pellet clad contact occurred, because a further increase in power would put the fuel into compressive loading and reduce tensile stresses. It was assumed that relative axial expansion only occurred until contact, whereupon a form of axial locking occurred. A typical analytically derived crack pattern is shown in Fig. 1 for a power of 12 kw/ft.

R-θ Model - The 2-dimensional R-θ model is shown in Fig. 2. This plane section represents material adjacent to a transverse crack and contains a symmetric section of a radial crack. The finite element mesh consists of 121 solid fuel and clad elements and 9 gap/friction elements. The number of radial cracks was varied parametrically because a unique number cannot be determined analytically based on fracture stress. Once the number is defined, however, the crack depth can be defined based on fracture stress. Axial locking is assumed in this model after contact although hoop friction forces are all that are allowed to transmit hoop loading.

The above models are applied over the range of 1 to 5 mils diametral gap and over a linear heat generation rate (LHGR) range of 6 to 16 kw/ft by imposing on the structural models (in a series of loading steps) the temperature distribution characterizing progressively higher LHGR's.

RESULTS - R-Z MODEL

Fig. 3 illustrates the contact patterns and ridging observed as LHGR is progressively increased for a typical pellet. At 10 kw/ft the pellet hourglassing is sufficient to cause contact only at the pellet ends, generating a small primary ridge in the clad at this point. At 12 kw/ft the hourglassing has increased and contact now occurs at the ends and at the midplane, increasing the primary ridge and generating a secondary ridge. It is noteworthy that the minimum clad diameter actually decreases slightly with the power increase from 10 to 12 kw/ft. Because of this, the ridge height (max minus min clad diameter at power) increases rapidly at powers just above initial contact. At higher powers, 14 to 16 kw/ft, the pellet and clad are fully in contact and the clad shape is defined by the pellet shape. Because of material softening and the higher interface loads at the pellet end, the maximum clad diameter increases progressively more slowly at high power, while the minimum diameter continues to increase at a significant rate. This leads to a decrease in primary ridge height for fuel irradiated to high power. Secondary ridging becomes more prominent in such situations, eventually nearly equaling the primary ridging in magnitude. Ridge heights eventually decrease at high powers. Because ridge height depends only on maximum and minimum hot clad dimensions, it does not correlate with maximum absolute clad strain (defined as $\Delta d_{hot}/d_{cold}$) or with maximum clad hoop stresses. For this reason, ridge height is inadequate as a measure of clad stress or strain concentration.

The ridging curves in Fig. 4 indicate that larger cold gaps produce more, rather than less, ridging at high power than do smaller gaps. This result is typical of many cases studied, and is explained as follows: Pellets with large gaps come into contact with the clad at higher powers than do those with small gaps and, therefore, are more hourglassed at the time of initial contact. However, the larger initial gap also produces less diametral clad strain and less hoop stress in the clad, for a given amount of ridging, than does the smaller gap. The lower clad stress level permits the more hourglassed large-gap pellet shape to persist at powers beyond that of initial contact, and the resulting greater clad ridge heights reflect this shape. Thus, clad ridge heights at high powers are greater for larger cold gaps because of the lower strain and stress in the clad in such cases. This result again emphasizes that clad ridging as commonly measured (maximum minus minimum diameter of the irradiated rod) is not proportional to maximum stress. The identical measured ridging can characterize any of several widely different stress states. To determine the actual stress (or strain) concentration in the clad, a knowledge of the absolute diametral strain is required.

Fig. 5 presents typical hoop, axial, and radial stress distributions in the inner clad elements (essentially the inner surface stresses in the clad) at the maximum and minimum powers shown in Fig. 4. The radial stress distributions exhibit high compression at areas of point contact, less compression in regions of continuous surfact contact, and zero stress in areas of no contact, all in accordance with expected behavior. The axial stress distribution at 10 kw/ft shows no net tension or compression in the bulk of the clad, consistent with pellet and clad uncoupled axially at this initial contact

power, and a tension/compression distribution near the interface plane, consistent with the bending of the clad in this region. At 16 kw/ft the axial stress distribution shows a net tension in the clad caused by the greater thermal expansion of the pellet, with pellet and clad in a "locked" condition. High compressive axial stresses are seen at both points of ridging where the clad is strongly concave inward, and peak tensile axial stresses are seen at points displaced slightly from the ridging planes where the clad is strongly concave outward. Hoop stress distributions are functions chiefly of the radial displacement except in the immediate vicinity of the ridges, where bending and local radial compression and resulting Poisson effects cause the point of maximum tensile hoop stress to be displaced axially from planes of maximum ridging.

Maximum (and average) clad hoop stress (strain) increase essentially monotonically with increasing LHGR at constant cold gap or with decreasing cold gap at constant LHGR as shown in Fig. 6.

Hoop stress concentration factors in the clad inner surface range from approximately 3.0 to 5.0 at the initial contact power, and decrease with increasing power to approximately 1.0 to 2.0 at 16 kw/ft (also shown in Fig. 6). Hoop stress concentration increases with increasing cold gap at constant LHGR, due to more localized contact forces for the larger cold gaps. Hoop strain and strain concentration factors show the same pattern. The existence of local plastic strains in the clad near the pellet ends leads to strain concentration factors somewhat larger than stress concentration factors.

RESULTS - R-θ MODEL

In the R-θ model, as LHGR is increased, radial cracks begin to open and cause the pellet region nearest the crack to expand more rapidly until contact with the clad occurs; thus creating a normal load concentration in the clad near the crack which persists even after full contact has occurred as LHGR is further increased. This, along with the frictional forces which concentrate a large interfacial shear load on the clad near the crack, are the most significant mechanisms which produce the typical stress distributions shown in Fig. 7. This figure shows hoop stress distributions on the clad inner surface for various LHGR, at a constant friction coefficient of 1.0 and a nominal 2 mil diametral gap.

The maximum and average clad inner surface hoop stresses increase monotonically with power, with the rate of increase decreasing slightly at high power due to material softening. Fig. 8 shows maximum and average hoop stress as a function of LHGR for several gap sizes and a constant friction coefficient of 1.0.

In general the hoop stress concentration near the crack is found to be sensitive to the friction coefficient, μ, between the pellet and clad due to differences in the amount of pellet-clad circumferential sliding which occurs as contact is made. Fig. 9 shows maximum and average hoop stress, as well as the concentration factor as a function of friction coefficient. Note that the reduction in stress concentration as μ decreases is caused both by a decrease in maximum stress and by an increase in average stress. This occurs

because the frictional shear forces between the pellet and clad generate compressive hoop components in the clad everywhere except at the crack location. Reduction of μ reduces these compressive components and thus increases the average tensile hoop stress in the clad.

Figure 10 shows the sensitivity of the concentration factor to friction coefficient, LHGR, and gap size. Because diametral interference is a function of cold gap, the average level of clad inner surface hoop stress is sensitive to cold gap. For a decrease of 1 mil in diametral gap, average hoop stress increases ~15 ksi. However, as shown in Fig. 10, the stress concentration factor is relatively insensitive to cold gap.

When results for various numbers of pellet radial cracks are compared in Fig. 11, both maximum (and average) hoop stress are found to be essentially independent of the number of cracks within the range analyzed (6 to 12 cracks). This is due to the high localization of hoop stress near the crack, so that the presence or absence of an additional crack beyond the locally affected material does not alter the magnitude of the stresses near the original crack. Also, this shows that the original relation of crack number versus power used in the R-θ model assumptions did not bias the results.

CONCLUSIONS

1. Clad ridges induced at pellet transverse cracks can exceed primary ridges. Evidence of the existence of the secondary ridges is supported experimentally.
2. Ridging is larger for larger gaps due to the increase in pellet distortion before contact.
3. Ridge heights, defined as maximum minus minimum diameter, are not good indicators of peak stress.
4. Stresses opposite radial cracks decrease rapidly away from the crack. Hence, the peak clad stresses are relatively insensitive to the number of radial cracks.
5. Peak clad stress adjacent to a pellet radial crack increases with increasing friction, but the average stress decreases.
6. Poisson's effect significantly reduces clad inner surface hoop stress at the pellet-pellet interface for the pellet analyzed. Therefore, the peak tensile hoop stress occurs slightly away from the interface.

REFERENCES

1. Fuel Rod Power Ramp Experiment, T. P. Papayoglou and H. W. Wilson, ANS Topical Meeting on Water Reactor Fuel Performance, May 9-11, 1977, St. Charles, Illinois.
2. AXISYM Finite Element Code: Modifications for Pellet-Cladding Mechanical Interaction Analysis, G. P. Engelman, CDAP-TR-78-041, October 1978.
3. Fuel-Clad Interaction: C-E Thermo-Structural Fuel Evaluation Methods, Combustion Engineering, Inc., CENPD-179 (non-proprietary version), April 1976.
4. Sensitivity of Power Ramp Induced Cladding Stress and Strain Concentrations to Modelling Assumptions, W. Hering, I. B. Fiero, and R. S. Darling, SMiRT-5 Conference Paper D-2/4.

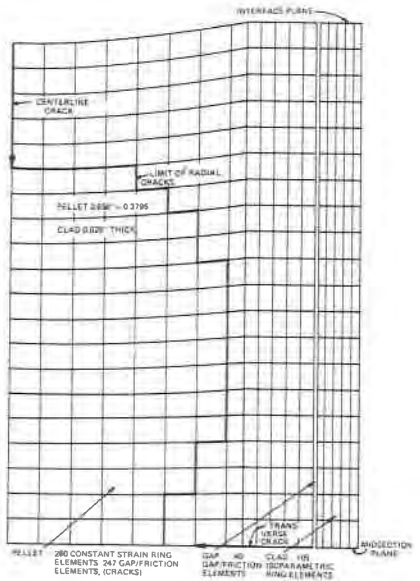

Figure 1
ANSYS R-Z FINITE ELEMENT MODEL

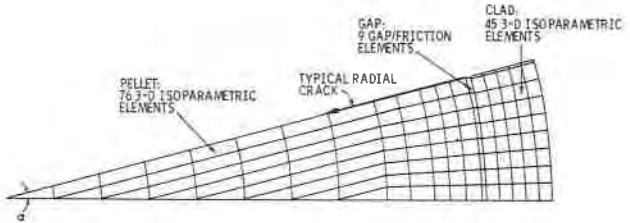

Figure 2
ANSYS R-θ FINITE ELEMENT MODEL

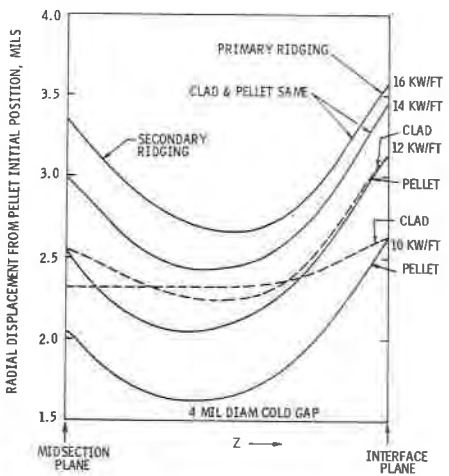

Figure 3
FUEL AND CLAD RADIAL DISPLACEMENT

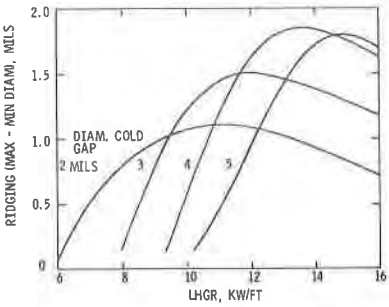

Figure 4
HOT CLAD RIDGING FOR TYPICAL PELLET

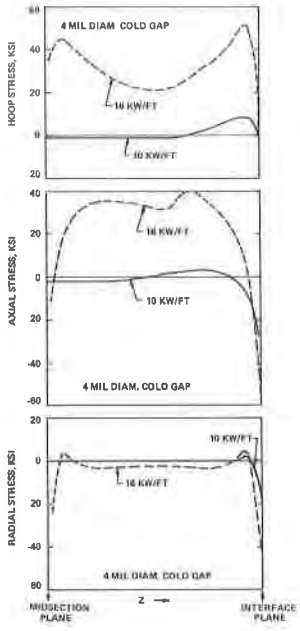

Figure 5
TYPICAL HOOP AXIAL, AND RADIAL STRESS DISTRIBUTIONS

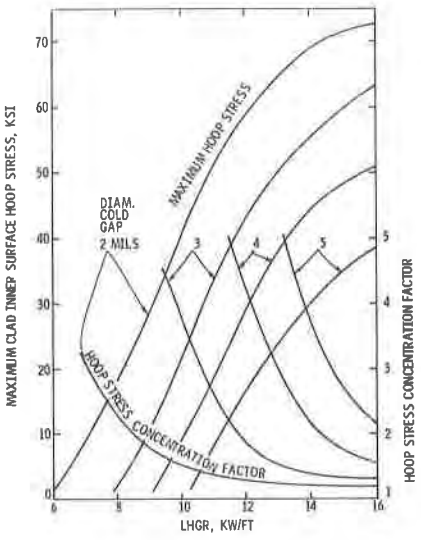

Figure 6
MAXIMUM HOOP STRESS IN CLAD INNER ELEMENTS
(R-Z MODEL)

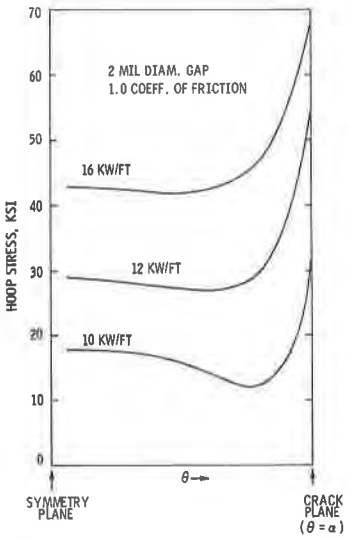

Figure 7
TYPICAL CIRCUMFERENTIAL HOOP STRESS DISTRIBUTION
IN CLAD INNER ELEMENTS

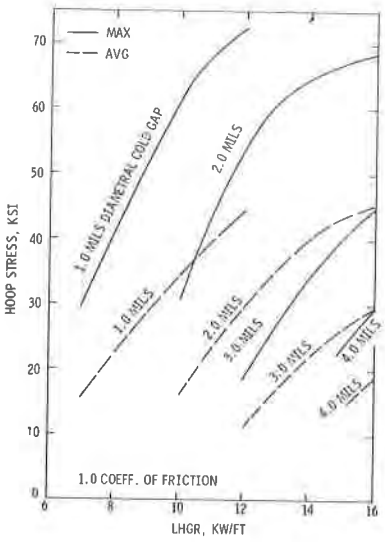

Figure 8
MAXIMUM AND AVERAGE CLAD
INNER ELEMENT HOOP STRESS
(R-θ MODEL)

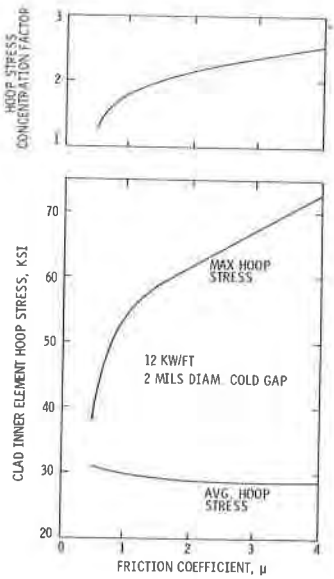

Figure 9
EFFECT OF COEFFICIENT OF FRICTION
ON HOOP STRESS
(R-θ MODEL)

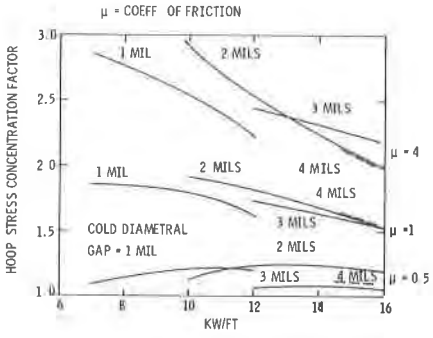

Figure 10
HOOP STRESS CONCENTRATION FACTOR
(R-θ MODEL)

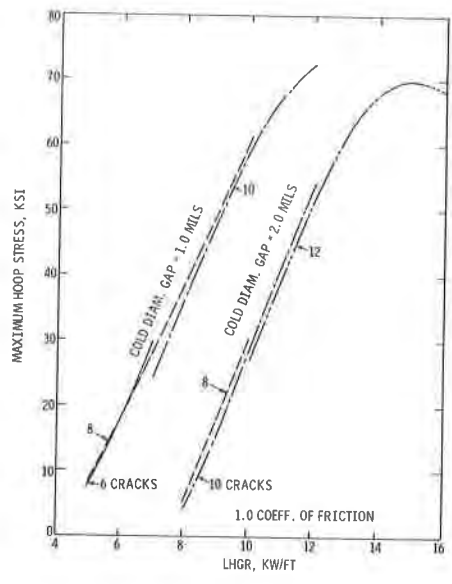

Figure 11
EFFECT OF NUMBER OF PELLET CRACKS ON
MAXIMUM CLAD INNER ELEMENT HOOP STRESS
(R-θ MODEL)